

# Kinematics of the ionized gas in the Local Group irregular galaxy IC 1613

M. Valdez-Gutiérrez<sup>1</sup>, M. Rosado<sup>2</sup>, L. Georgiev<sup>2</sup>, J. Borissova<sup>3</sup> and R. Kurtev<sup>4</sup>

<sup>1</sup> Instituto Nacional de Astrofísica, Óptica y Electrónica, Calle Luis Enrique Erro 1, 72840 Tonantzintla, Puebla, México

<sup>2</sup> Instituto de Astronomía, Universidad Nacional Autónoma de México, México

<sup>3</sup> Institute of Astronomy, Bulgarian Academy of Sciences and Isaac Newton Institute of Chile Bulgarian Branch, 72 Tsarigradsko chaussée, BG –1784 Sofia, Bulgaria

<sup>4</sup> Department of Astronomy, Sofia University and Isaac Newton Institute of Chile Bulgarian Branch, BG –1164 Sofia, Bulgaria

Received 7 June 2000 / Accepted 20 September 2000

**Abstract.** We present H $\alpha$  and [SII] observations for the Local Group irregular galaxy IC 1613 using the PUMA scanning Fabry–Perot interferometer. Our goal is to analyze the kinematics of the ionized gas in the complex sample of superbubbles located in the whole extension of our field (10'), which includes most of the optical emission of this galaxy, and to study the inter-relationship between young stellar associations and nebulae based on a previous study that we have made on the stellar associations of the central region of this galaxy. The ionized gas in this galaxy is distributed in classical H II regions and in a series of superbubbles (also called giant shells) covering a large fraction of the optical extent of the galaxy.

We present a catalog of kinematical properties of both the H II regions of this galaxy and the superbubbles. We have also compared the kinematics of the ionized gas in H II regions to search for possible dynamic differences between neutral and ionized gas.

**Key words:** Galaxies: irregular – Galaxies: individual: IC 1613 – Galaxies: kinematics and dynamics – Local Group – (ISM): HII regions – ISM: bubbles

## 1. Introduction

Irregular galaxies constitute a substantial fraction of all galaxies. They are also dominant among the actively star-forming galaxies. Because they lack spiral density waves, they are excellent laboratories to examine the star formation process in alternative scenarios. Also, they can provide important clues about the mechanisms of formation of “bubbles” (the ring-shaped nebulae with diameters,  $D \lesssim 50$  pc), “superbubbles” or “giant shells” (ring-shaped structures with  $D \lesssim 400$  pc) and “supershells” (ring-shaped structures with  $D \approx 1$  kpc). Massive stars can dramatically change the interstellar medium (ISM)

of these galaxies by means of supernova explosions and stellar winds. On the other hand, the ISM content and energetics can have important effects on the subsequent mechanisms of star formation. Indeed, the compressions produced by shocks formed by supernova explosions or powerful stellar winds on the molecular clouds could trigger the formation of a second generation of stars at the edges of the shells formed by these events (self-induced star formation).

The Local Group irregular galaxies are exceptional targets for the study of the inter-relationship between gas and stars because they are easily resolved. This means that we could know the stellar content of nebular H II complexes and superbubbles and try to identify for relationships between the interior stellar associations and the dimensions and kinematics of the superbubbles. This kind of investigation has been performed for the most favorable case, the Large Magellanic Cloud (Rosado 1986; Oey 1996a, 1996b, amongst other references). Indeed, it is in this galaxy that a clear example of self-induced star formation has been found: the nebular complex N11 (Parker et al. 1996; Rosado et al. 1996).

In this work, we study the nebulae and massive stellar content of the nearby irregular galaxy: IC 1613. This galaxy belongs to the Local Group and it is located at a distance of 725 kpc (Freedman 1988a, 1988b). Table 1 reviews some of its main properties. Because of its proximity, it has been the target of several studies. Its stellar content has been analyzed by Baade (1963), Sandage (1971), Sandage & Katem (1976), Hodge (1978, 1980), Freedman (1988a, 1988b) and Georgiev et al. (1999; hereafter Paper I). Several candidate Wolf-Rayet (WR) stars were detected but only one of them was spectroscopically confirmed over the whole extent of this galaxy (Azzopardi et al. 1988; d’Odorico & Rosa 1982; Kingsburgh & Barlow 1995). This WR is a WO-type star embedded in a large nebular complex located at the southern region of this galaxy (Rosado et al. 2000). The H II regions of IC 1613 have been studied by Sandage (1971), Hodge et al.

(1990; hereafter HLG), Price et al. (1990) and Hunter et al. (1993). The peculiarity of the kinematics of some of the superbubbles of ionized gas has been analyzed by Meaburn et al. (1988). Their work focused only on the NE region of the galaxy where bright H II complexes are easily detected. Other spectroscopic studies on the nebulae of IC 1613 mainly examine the only SNR (d’Odorico et al. 1980; Peimbert et al. 1988; Dickel et al. 1985; Goss & Lozinskaya 1995; Rosado et al. 2000). The distribution of the H I gas in IC 1613 has been analyzed by Lake & Skillman (1989). These authors have found that the H I content makes up to 20 percent of the total mass (see also Huchtmeier et al. 1981).

In this work, the results of our kinematic analysis, making use of a scanning Fabry-Perot interferometer (PUMA, Rosado et al. 1995), are presented. We analyze the relationship between nebulae and the stellar associations studied in Paper I. The observations and data reductions are described in Section 2. In the remaining sections we study the kinematic behavior of the H II regions and superbubbles. In Section 3 we show the nebulosities of this galaxy in several emission lines. We also indicate how our photometric calibration has been done. In Section 4 we study the kinematics of H II regions and superbubbles in IC 1613. We obtain the peak velocities and velocity dispersions of the H II regions, as well as their stellar content. We also obtain the H II luminosity function and diameter distribution. In Section 5 we study the superbubbles found, obtaining their dimensions, expansion velocities, H $\alpha$  fluxes and studying their stellar content. We also obtain some important physical parameters of the superbubbles and the superbubble diameter distributions. We analyse the possibility that the superbubbles were formed by the combined action of stellar winds and supernovae explosions. In Section 6 we present the radial velocity field in our field of view, obtained from diffuse ionized gas, H II regions and superbubbles. We compare our trends with the results of H I observations. In Section 7 we present our conclusions.

## 2. Observations and data reduction

The observations were carried out during the nights of December 5 and 6, 1996 and November 15, 1998 with the UNAM Scanning Fabry-Perot interferometer PUMA attached to the f/7.9 Ritchey-Chretien focus of the 2.1 m telescope at the Observatorio Astronómico Nacional at San Pedro Mártir, B.C., México.

The PUMA setup was composed of a scanning Fabry-Perot interferometer (SFPI), a focal reducer with a f/3.95 camera, a filter wheel, a calibration system and a Tektronix 1K $\times$ 1K CCD detector (Rosado et al. 1995). Table 2 reports the main characteristics of the instrumental setup.

We obtained a series of direct images in the lines of H $\alpha$ , [S II] ( $\lambda$  6717 and 6731 Å) and [O III] ( $\lambda$  5007 Å) using the PUMA in its direct image mode (without the SFPI). The exposure times of each of the direct images were 60 s, 60

s and 300 s for the H $\alpha$ , [S II] and [O III], respectively. The CCD reading was binned 2 $\times$ 2, giving a pixel size of 1'17 (equivalent to 4.21 pc at the adopted distance) and a field of view covering 10' including the NE region and several other interesting regions of IC 1613.

In addition, we obtained scanning FP interferometric data cubes in the lines of H $\alpha$  and [S II] ( $\lambda$  6717 and 6731 Å). The H $\alpha$  cubes share the same scale and field of view as the direct images. Given that the [S II] intensities were lower than the H $\alpha$  intensities, we binned 4 $\times$ 4 the CCD reading of the [S II] cubes and correspondingly, we obtained a pixel size of 2'34.

The phase calibration was made by taking data cubes of a calibration lamp before and after the galaxy exposure. We used a hydrogen lamp for calibrating the H $\alpha$  nebular cubes and a neon lamp for calibrating the [S II] nebular cubes. Since the redshift of this galaxy is not high, phase corrections, due to the difference in wavelength between the galaxy and the calibration line, are not required.

The FP data cubes are composed of 48 steps, with integration times of 60 seconds per step. In this form, the final data cube dimensions in H $\alpha$  and [S II] were 512 $\times$ 512 $\times$ 48 and 256 $\times$ 256 $\times$ 48, respectively. For the H $\alpha$  observations we obtained 4 data cubes that were summed giving a total exposure time of 3.2 hours. For the [S II] observations we obtained 3 data cubes that also were summed, with a total exposure time of 2.4 hours.

Reductions were carried out using the software package CIGALE (Le Coarer et al. 1993). Our data cubes in H $\alpha$  are contaminated with line-sky emission such as the geocoronal H $\alpha$  line and the lines of OH at 6577.18 Å and 6577.38 Å, respectively. The night-sky lines fell well outside the main emission of IC 1613, due to the systemic velocity of this galaxy. These night-sky lines were subtracted using an interactive routine of CIGALE. The data cubes in the [S II] lines are less contaminated by line-sky emission; however, the S/N ratio is not as good as that of the H $\alpha$  cubes and so will be used only for comparison.

To extract the kinematic information from the FP data cubes we proceeded in different ways for the H II regions and for the superbubbles. In the case of the H II regions, we obtained only one radial velocity profile at H $\alpha$ , integrated over a box containing the whole H II region. In the case of the superbubbles, we proceed in a different way in order to seek for internal motions revealed by line splitting of the velocity profiles. We obtained the radial velocity field of the superbubble by dividing the superbubble dimensions into several small boxes over which we obtained several radial velocity profiles, both in H $\alpha$  and [S II].

The radial velocity profiles were fitted by Gaussian functions after deconvolution by the instrumental function (an Airy function). We constructed a map of the monochromatic (continuum) emission by integration of the radial velocity profile of each pixel, up (down) to a certain fraction of the peak. This map enabled us to separate the monochromatic emission from the continuum (Le

Coarer et al. 1993). To get the radial velocity map of our observed field, we found the central velocity in the radial velocity profile of each pixel, that has a level above  $2\sigma$  the value of the standard background emission, to ensure galaxy membership.

### 3. Morphology of the nebulae in IC 1613

Figure 1 shows the emission of IC 1613 in the lines of  $H\alpha$ , [S II] and [O III] as obtained from our direct images. The photometrical center of IC 1613 is located at RA(1950)=01:02:19.6 and Dec(1950)=+01:51:56.1 (Mateo 1998). The most active region of IC 1613 is located  $3'$  (or 663 pc) North-East from the photometric center. Hereafter, we will call this quadrant the NE region. Bright H II regions, bubbles and superbubbles are situated in the NE region. Numerous H II regions and larger structures, some of them ring-shaped, are superimposed over the extent of the chaotic body of the galaxy. Except for the bright network of superbubbles located in the NE region of the galaxy, the nebulae are weaker in the [S II] lines and they do not show any appreciable [O III] emission.

In the South of this rich sector of the galaxy (at  $3'8$  or 838 pc from the center), there is a giant H II region (Sandage 3). Southwest of the center of the galaxy at  $2'4$  (535 pc) we located the H II region Sandage 2.

#### 3.1. The H II region content

The H II regions of IC 1613 have been catalogued by Sandage (1971), Lequeux et al. (1987), Price et al. (1990) and HLG (who catalogued 77 H II regions, reporting their diameters and  $H\alpha$  fluxes).

Our observed field contains 44 diffuse nebulae according to HLG. The limits of each H II region or group of H II regions were defined by the contour where the intensity of the  $H\alpha$  emission falls to the average local intensity of the diffuse background. However, in some cases, the boundaries between diffuse H II regions are not obvious. In addition, we were not able to resolve some regions. In these cases, we assign to them a common boundary, and, consequently, only 30 regions were clearly defined.

#### 3.2. Photometric calibration

We calibrate our monochromatic  $H\alpha$  image in flux, using the measurements of HLG. Eight isolated and round regions were selected from HLG lists (Table 3). For each region we measured the flux of our monochromatic  $H\alpha$  image, using apertures with the same equivalent area as in HLG. A least squares fit to the data gives a conversion factor of 1 count  $s^{-1}$  (in our  $H\alpha$  image) =  $6.26 \cdot 10^{-18}$  erg  $cm^{-2} s^{-1}$ . We preferred a conversion factor per unit area for easy calculations of the flux in irregular H II regions and superbubbles. Polygonal apertures were chosen such that they must contain all emission from a given H II

**Fig. 1.** Top to bottom: Direct images of IC 1613 in  $H\alpha$ , [S II] and [O III], respectively. The exposure time is 60 sec for  $H\alpha$  and [S II], while for [O III] it is 300 sec (see text for details). The scale and the orientation are indicated in the upper panel.

region or superbubble. Pixels within the apertures were summed to generate the total H II region or superbubble plus background counts. The background emission was computed using apertures with the same area as the ob-

ject, as close to the object as possible. The total H $\alpha$  flux for every H II region and every superbubble was obtained when the background was subtracted and the resulting counts multiplied by the conversion factor. H $\alpha$  fluxes are presented in column 9 of Table 4 for the H II regions and column 6 of Table 6 for the superbubbles. Figure 2 shows the comparison between our measurements and HLG for the common HII regions not included as calibrators.

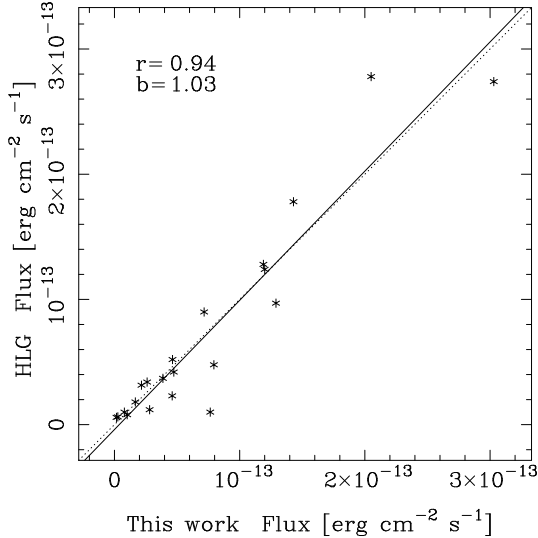


**Fig. 2.** Comparison between our flux determinations and HLG fluxes. The calibrator HII regions were not used in the fitting. The values of the correlation coefficient ( $r$ ) and the slope ( $b$ ) are given to the left. The dotted line is our best fit, and the solid line is the diagonal.

#### 4. Kinematics of the H II regions in IC 1613

Figure 3 shows the H $\alpha$  monochromatic image of IC 1613 (continuum subtracted) obtained from our FP cubes using the method described in Section 2. Superimposed on this image, we marked the rectangular boxes over which the radial velocity measurements of the observed H II regions were performed. We obtained radial velocity profiles of these sources by integrating in those rectangular boxes. We will refer to these profiles as “integrated” because they are obtained by integrating over the whole extent of the H II region. Also, in this figure, we marked with asterisks the WR star candidates (Armandroff & Massey 1985). Only one of these candidates was confirmed as a WR star; another was confirmed as the SNR Sandage 8 and the remaining were identified as OB stars (Azzopardi et al. 1988).

The integrated radial velocity profiles are, in general, single for all the H II regions; in this case, a single Gaussian function was fitted as described above. In only two cases: the SNR Sandage 8 (our source N18, see Table 4) and the giant shell Sandage 10/13 (N27), the integrated radial velocity profiles were complex. In those cases, we carried

out a profile decomposition into two Gaussian functions. We then list the two velocity components obtained from our profile fitting. A more detailed study of the kinematics of S8 from the FP data will be given elsewhere (Rosado et al. 2000). Also, a more detailed study of the internal kinematics of the superbubble N27 = 67 (HLG) and of other superbubbles in this galaxy is given in the following section.

Table 4 gives a catalogue of the kinematical parameters of the H II regions of IC 1613, within the field of view of our observations. It is important to note that some of the objects listed in this table are ring-shaped and consequently are better classified as superbubbles and will be studied in more detail in the following section. We include these objects in Table 4 because they appear in previous catalogues (Sandage 1971 and HLG) but we exclude them from the calculation of the H II region luminosity function and diameter distributions.

In Table 4, we have listed the name (adopting both HLG’s and Sandage’s conventions), diameter (see the definition for this parameter in Section 4.2), peak velocity and velocity dispersion from the Gaussian fitting to the radial velocity profile, and the H $\alpha$  flux, derived as described in Section 3.2. To obtain luminosities, our fluxes were corrected only for galactic foreground extinction using the  $A_B=0.21$  mag value given in the RC2 catalog (de Vaucouleurs et al. 1976). The effects of internal extinction in these determinations seems to be not crucial (Hippelein 1986). The radial velocities were corrected to the heliocentric system of reference. Our dispersions ( $\sigma_{obs}$ ) have been corrected for instrumental ( $\sigma_{inst}$ ), thermal ( $\sigma_{th}$ ) and intrinsic ( $\sigma_{intrin}$ ) broadenings respectively, according to:

$$\sigma_{corr}^2 = \sigma_{obs}^2 - \sigma_{inst}^2 - \sigma_{th}^2 - \sigma_{intrin}^2$$

where  $\sigma_{inst} = 43.5$  km s $^{-1}$ ,  $\sigma_{th} = 9.1$  km s $^{-1}$  for hydrogen gas at  $T_e=10^4$  (Spitzer 1978) and  $\sigma_{intrin} = 3$  km s $^{-1}$  for the fine structure of the H $\alpha$  line. Some authors also refer to  $\sigma_{corr}$  as the turbulent velocity dispersion.

An inspection of this table shows that the heliocentric radial velocities range from  $-228$  to  $-254$  km s $^{-1}$ . The equivalent diameters range from 27 pc (corresponding to region N24) to 253.6 pc (for region Sandage 3 or N9) and their mean value is around 82 pc. The corrected velocity dispersions are supersonic for most of the objects with values ranging from 16 to 35 km s $^{-1}$  with a mean value of 20 km s $^{-1}$ . Some H II regions have low S/N ratios and consequently their determinations of peak velocity and velocity dispersion are uncertain. These cases have been quoted within parentheses in Table 4. The H $\alpha$  fluxes range from  $1.60 \times 10^{-15}$  to  $9.24 \times 10^{-13}$  ergs cm $^{-2}$  s $^{-1}$ ; these lower and upper limits correspond to the H II regions N13 and N27, respectively.

In Table 5 we give the stellar content in order to identify the exciting star or stars that are related to the analyzed H II regions. Column 1 gives the identification labels

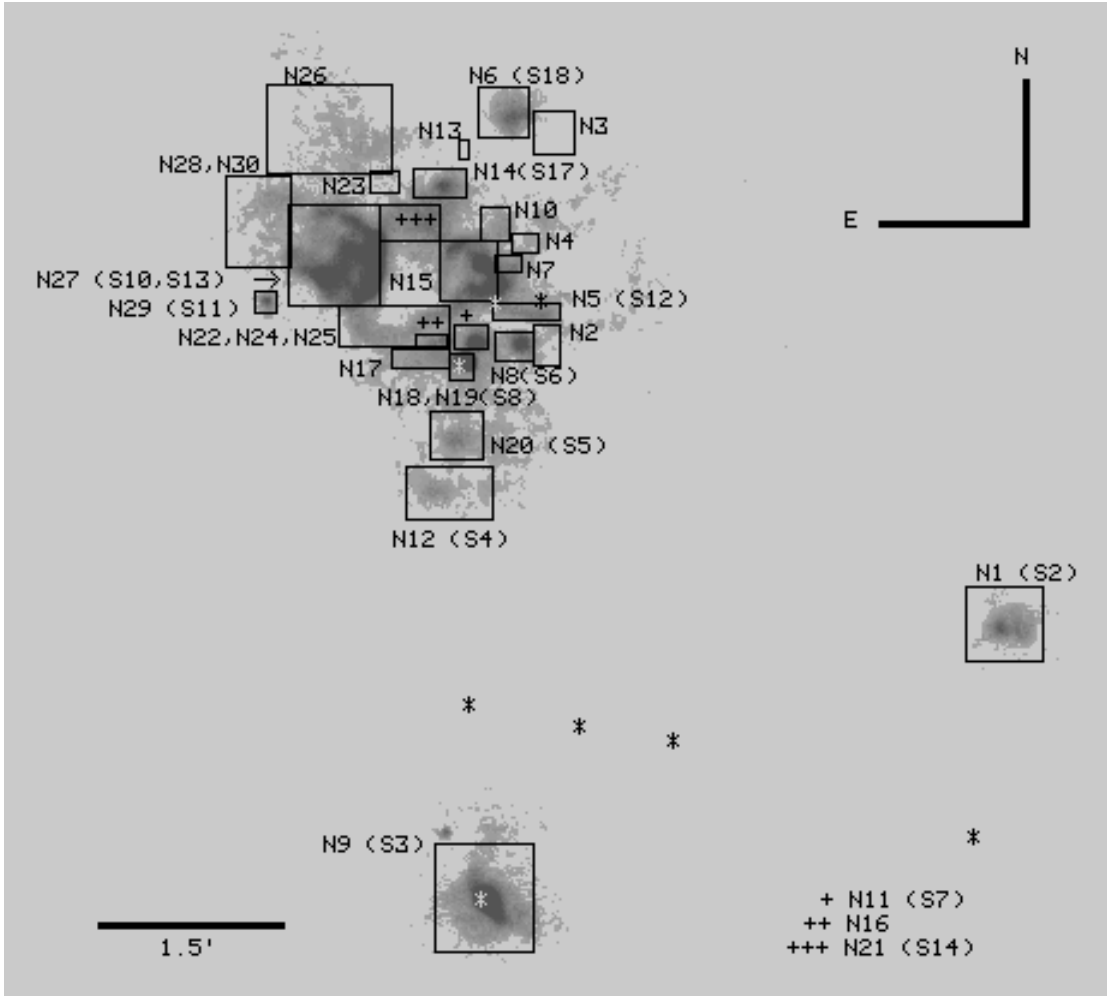


**Fig. 3.**  $H\alpha$  monochromatic image of IC 1613. The background has been subtracted at  $2\sigma$  its mean value in order to reveal the weaker features. The boxes correspond to places where the kinematical analysis was performed. Sandage identifications have been quoted between parentheses if relevant. The asterisks indicate positions for the eight WR star candidates (Armandroff & Massey 1985). Some labels are denoted with crosses, at the left bottom of the figure. The scale and orientation are indicated to the left and right, respectively. In this Figure the field covers approximately  $9' \times 9'$ .

used in this work. Column 2 and 3 list the WR candidates (Armandroff & Massey 1985) that coincide with some of our H II regions and their spectral type (or related object) according to Azzopardi et al. (1988). Columns 4, 6 and 7 indicate the stellar associations and clusters determined in previous works. All but four H II regions have an evident stellar content that is probably the source of the UV flux.

#### 4.1. The H II region luminosity function

Figure 4 shows the  $H\alpha$  luminosity function for the H II regions in IC 1613. For several galaxies, it has been shown that the brighter luminosity end of the H II region luminosity function can be fitted with a power law in the form:  $N(L) = AL^a dL$ , where  $N$  is the number of H II regions with luminosity  $L$  in an interval of luminosity  $dL$ , and the

slope  $a$  is related to the morphological type of the galaxy (Kennicutt et al. 1989), ranging from mean values of  $-2.3$  (Sab-Sb galaxies) to  $-1.75$  (Irregulars). It also has been suggested that different ranges of the luminosity function are related to different kind of objects, such as H II regions ionized by single stars and those ionized by clusters of stars (Hodge et al. 1989; Youngblood & Hunter 1999).

To obtain the H II region luminosity function we take the logarithm of the number of H II regions divided by the corresponding luminosity bin width (0.26 dex in our calculation). The bin width was chosen in terms of our relatively small number of objects (30 H II regions) and the fit was calculated to the bins brighter than  $\log L = 36.5$ . Our best fit slope for IC 1613 gives  $a = -1.54 \pm 0.1$ . This value is similar to the value ( $a = -1.6 \pm 0.2$ ) found by HLG, and is within the mean values found for a sample

of irregular galaxies studied by Kennicutt et al. (1989), Strobel et al. (1991), Kingsburgh & McCall (1998) and Youngblood & Hunter (1999).

#### 4.2. The H II region diameter distribution

We measured the diameter of the H II regions on the monochromatic H $\alpha$  image and they are reported in column 4 in Table 4. The reported diameter is the equivalent diameter, which is defined as  $D = (4A/\pi)^{1/2}$ . In this definition,  $A$  is the area of the apertures wherein the photometry was performed. The measured diameters range from 27 to 254 pc (this later value corresponds to large H II complexes that are not ring-shaped).

The cumulative H II region diameter distribution  $N(> D)$  has been calculated and in Figure 5 we plot  $\log N(> D)$  vs  $D$ . This functional dependence was proposed by van den Bergh (1981) as a universal law for all galaxy types and it has been used to study the statistics of the H II region populations in combination with the H II region luminosity function. The slope in the cumulative H II region diameter distribution is related to the characteristic diameter  $D_0$  of the H II regions in a galaxy. For IC 1613, a least squares fit gives  $D_0 = 65.41 \pm 3$  pc. This value is marginally in agreement with a previous one determined by HLG who obtained  $D_0 = 56$  pc. However our value differs from that of Price et al. (1990) who quoted a larger value ( $D_0 = 83$  pc). This discrepancy can be easily explained, because Price et al. (1990) also considered some superbubbles in their calculation (see Section 5). Looking for other correlations, Hodge (1983), using a sample of 18 irregular and related galaxies (IC 1613 was not in his sample), found a good correlation between the characteristic diameter  $D_0$  and the absolute magnitude  $M_B$  of a galaxy. In a subsequent work, Strobel et al. (1991) increased the sample of Hodge (1983) with 7 additional galaxies (IC 1613 was also not included in these new objects). They found that the previous correlation between  $D_0$  and the absolute magnitude  $M_B$  becomes weaker, having the form  $\log D_0 = 0.25(\pm 0.29) - 0.098(\pm 0.017)M_B$ . For IC 1613 this relation gives a value of  $\log D_0 = 1.64$  – taking  $M_B = -14.2$  from Mateo (1998) – in agreement with our calculation ( $\log D_0 = 1.83$ ). However, if we plot our resulting  $D_0$  in Figure 11 in Strobel et al. 1991, our data point falls outside the line fit in that plot, a fact that points towards the conclusion given by Strobel et al. (1991). In that sense, in a more recent work, Youngblood & Hunter (1999), using a sample of 29 irregular and Blue Compact Dwarfs (IC 1613 not included), have shown that this correlation is indeed a very weak one (see their Figure 9).

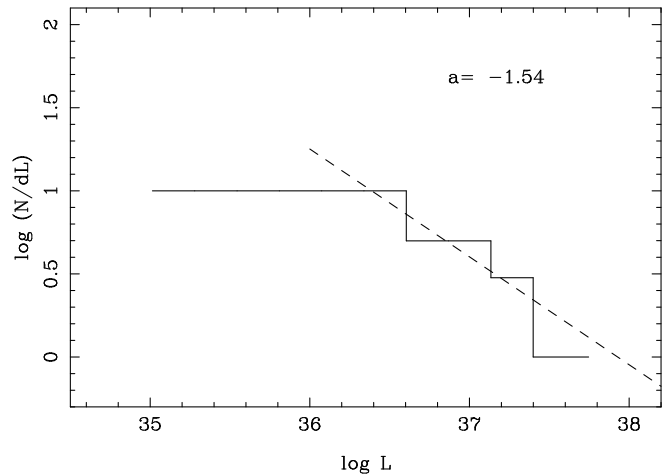


**Fig. 4.** The H $\alpha$  luminosity function for the H II regions in IC 1613. The dashed line is the least squares fit to a power law. The slope value is given to the right.

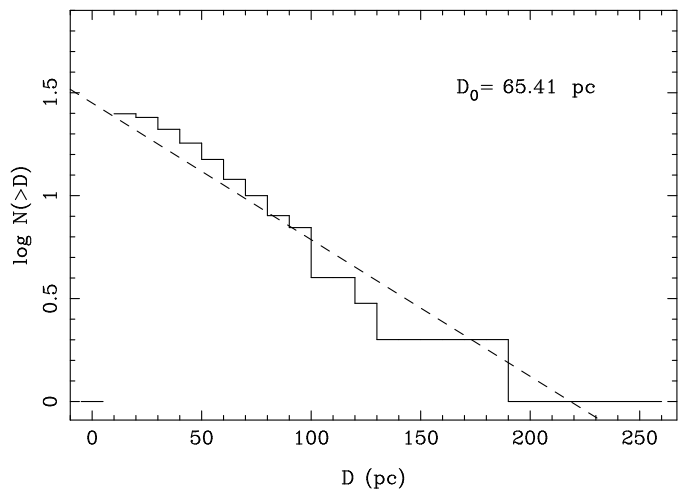


**Fig. 5.** The cumulative size distribution for the H II regions in IC 1613, where the dashed straight line is a least squares fit. The value for the characteristic diameter is given to the right.

## 5. Kinematics of the superbubbles (giant shells) of IC 1613

Figure 6 shows one of the velocity maps (at  $V_{helio} = -234$  km s $^{-1}$ ) of the H $\alpha$  emission of IC 1613, obtained from our FP observations. The contrast of this image is higher than the direct image shown in Figure 1 because the FP interferometer acts as a filter with a very narrow width (0.41 Å) while the bandwidth of the filter used to obtain the direct image in Figure 1 is 20 Å. Thus, it allows the detection of the line emission from the galaxy while reducing spurious line or continuum emission. Furthermore, in order to enhance the detection of low emissivity features of large dimensions, this velocity map was smoothed spa-

tially using a Gaussian filter of 4 pixels width in both X and Y axis.

We note that the entire observed field is covered by networks of shells, rings and filaments whose diameters range from 110 pc (30''6) to 325 pc (90''6). We will follow the terminology of this type of structures given in the introduction. In accord with this terminology, Figure 6 shows that the entire field of our observations of IC 1613 is covered by superbubbles. We were able to differentiate 17 large diameter ring-shaped structures. The rough location of these superbubbles are marked on Figure 6. We detect the seven superbubbles or giant shells, GS, (from GS1a and b to GS6) already reported by Meaburn et al. (1988), as well as several others located outside the field (to the S and to the W) covered by Meaburn et al. (1988). Most of the newly detected superbubbles lie outside the bright NE region of the galaxy and they are very faint and difficult to visualize. Some of them are coincident with the H II regions and filaments reported by Price et al. (1990) and Hunter et al. (1993).

Figure 7 and Figure 8 show some of the H $\alpha$  and [S II] velocity maps (or channels) where the network of superbubbles in the NE region is clearly appreciated. The heliocentric radial velocities for these superbubbles range from  $-100$  to  $-350$  km s $^{-1}$ . The superbubbles appear different in the several FP velocity maps, allowing us to disentangle several of them that appear superimposed in the direct images. In particular, the giant shells 1a and 1b of Meaburn et al. (1988) (corresponding to superbubbles R1 and R2, respectively) appear in different velocity channels: R1 (Meaburn's GS 1a) is better visualized in channels covering heliocentric velocities from  $-272$  to  $-253$  km s $^{-1}$  (and even more negative velocities not shown in the figures), whereas R2 (Meaburn's GS 1b) is better appreciated in channels where the heliocentric velocity ranges from  $-234$  to  $-196$  km s $^{-1}$ .

In order to quantify the relative importance of the superbubbles and to compare with other galaxies, we have calculated the 2-D porosity parameter,  $Q_{2D}$ , in our field, defined as the ratio of the total area occupied by the catalogued superbubbles to the total area of the galaxy seen in our field of view (Oey & Clarke 1997). We obtain  $Q_{2D} = 0.75$ , a value that is intermediate between the observed  $Q_{2D}$  values for the SMC (1.6) and M 31 (0.01) according with Oey & Clarke (1997). However, the  $Q_{2D}$  of the whole galaxy must await observations of the type described in this work covering the whole dimension of IC 1613.

According to the procedure discussed at the end of Section 2, we obtained the radial velocity field of the superbubbles. We used mainly the H $\alpha$  data; however, we used also the [S II] data for the superbubbles which showed bright emission in the [S II] lines. Some of the superbubbles of the NE region appear also in Table 4. In that table we have only quoted the velocity values extracted from the integrated radial velocity profiles, while in the following

we will use the radial velocity field in seeking for internal motions.

Figure 9 shows, as an example, the radial velocity profile of one of the superbubbles where the splitting is clearly visible. As we can see from this figure, some of the profiles are complex and require to be fitted by a superposition of at least two Gaussian functions. We interpret the different components as being due to an expansion motion. Table 6 gives a catalogue of the detected superbubbles, their identification (if any) according to Meaburn et al. (1988), Price et al. (1990) and Hunter et al. (1993, hereafter HHG), their angular dimensions, the peak heliocentric velocities of the Gaussian functions fitted to the velocity profile and the calibrated H $\alpha$  fluxes and luminosities. The last column of Table 6 corresponds to comments on the morphology of the superbubbles. We have found that some of the superbubbles have the "ring of H II regions" structure (i.e., the shell has smaller H II regions at its boundaries). This morphological type presents some evidence of shock-induced star formation as Rosado et al. (1996) have found for superbubbles in the LMC.

### 5.1. The stellar content of the superbubbles

The superbubbles catalogued in Table 6 are directly related to the stellar associations of IC 1613. These stellar associations were catalogued by Hodge (1978) for the entire galaxy. In Paper I, we have studied the stellar content of the NE region of the galaxy and applied an automatic method to obtain the boundaries of the stellar associations. Figure 10 shows the stellar associations studied in Paper I, where the superbubble boundaries shown in Figure 6 are also marked. We see that there is a good agreement between the locations of most of the stellar associations and the centers of the superbubbles. For the superbubbles outside the NE region we also find a good agreement between the positions of Hodge's (1978) associations and the superbubbles.

The stellar associations within the superbubbles boundaries are reported in Table 7. In this table we have listed (1) the superbubble's number (according to our catalogue), (2) the Paper I and Hodge's (1978) stellar associations located within the superbubble boundaries, (3) the number of blue stars of the interior associations (stars with  $M_v < -2.0$ ,  $(B - V)_0 < 0.0$  and  $(U - B)_0 < -0.5$ , corresponding to stars with masses larger than  $7 M_{\odot}$ , (4) the age of the stellar associations, the possible existence of (5) OB stars and (6) blue supergiants with known spectral types and (7) the  $\Gamma$  exponent of the Initial Mass Function of the interior associations. Columns 3, 4, 6 and 7 were derived from the data published in Paper I. Column 5 is based on the spectra published for several Wolf-Rayet (WR) star candidates in this galaxy (Armandroff & Massey 1985, Azzopardi et al. 1988). An examination of this table shows that the stellar associations reported in Paper I have a better correlation with the catalogued su-

**Fig. 6.** Velocity map (at  $V_{helio} = -234 \text{ km s}^{-1}$ ) of the  $H\alpha$  emission of IC 1613, obtained from the scanning FP observations. Superimposed on this map are the boundaries of the 17 superbubbles catalogued in Table 6.

perbubbles than Hodge's. This is because Hodge's (1978) associations are, in general, larger than those reported in Paper I. Given that so many of them are interior to the superbubbles, we can conclude that the method of identification of stellar associations discussed in Paper I works very well. We also see that every catalogued superbubble can be associated with a relatively young stellar association (except R4, which probably has an older interior association), even the dimmer superbubbles, located far away from the bright NE region of IC 1613. This suggests that the interior associations are responsible for the formation of the superbubbles.

### 5.2. Physical parameters of the superbubbles

From the observed data (listed in Table 6) we can extract several physical parameters of the superbubbles:

1. The rms electron density of a superbubble is calculated from its  $H\alpha$  flux and dimensions according to the relation:

$$n_e^2(\text{rms}) \text{ (cm}^{-6}\text{)} = 2.74 \times 10^{18} \text{ F(H}\alpha\text{) R}^{-1} \theta^{-2}$$

This relation was obtained by assuming that the emitting gas is at  $T = 10^4 \text{ K}$  and distributed in an spherical shell of radius  $R$  (in pc) and thickness,  $\Delta R = R/12$ . The other quantities,  $F(H\alpha)$  and  $\theta^2$ , are listed in Table 6.

2. The expansion velocity,  $V_{EXP}$ , of a superbubble can be estimated as one half of the difference in velocities of the components listed in Table 6.

3. The mechanical energy of the superbubble,  $\text{K.E.} = 0.5 M V_{EXP}^2$ , is calculated according with the relation:

$$\text{K.E. (ergs)} = 1.7 \times 10^{41} n_e(\text{rms}) \text{ (cm}^{-3}\text{)} V_{EXP}^2 \text{ (km s}^{-1}\text{)} R^3$$

In obtaining this relation we have assumed that the mass is concentrated in the spherical shell of radius  $R$  (in



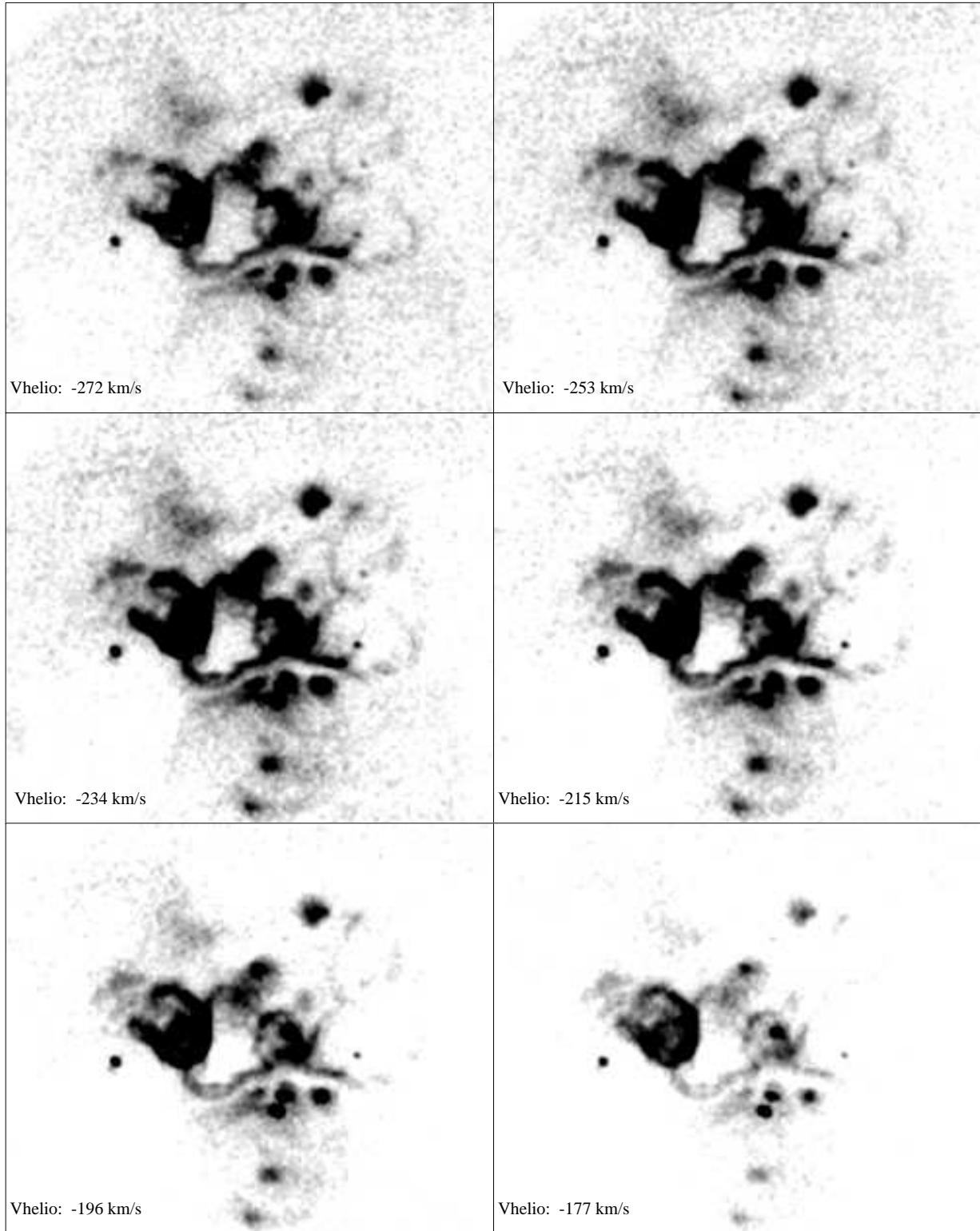


**Fig. 7.**  $H\alpha$  velocity maps of the NE region in IC 1613 where the superbubble network appears bright. In this map, the superbubbles R1, R2, R4, R5, R6, R7, R8, R9, R10 and R13 are more clearly visible because of the high contrast of the print.

pc) and thickness,  $\Delta R = R/12$ . We have also assumed that  $\mu = 0.65$ , as for an ionized hydrogen gas.

4. The kinematic age of the superbubble can be obtained from the following relation:

$$t(\text{yr}) = 4.8 \times 10^5 R/V_{EXP} (\text{km s}^{-1})$$

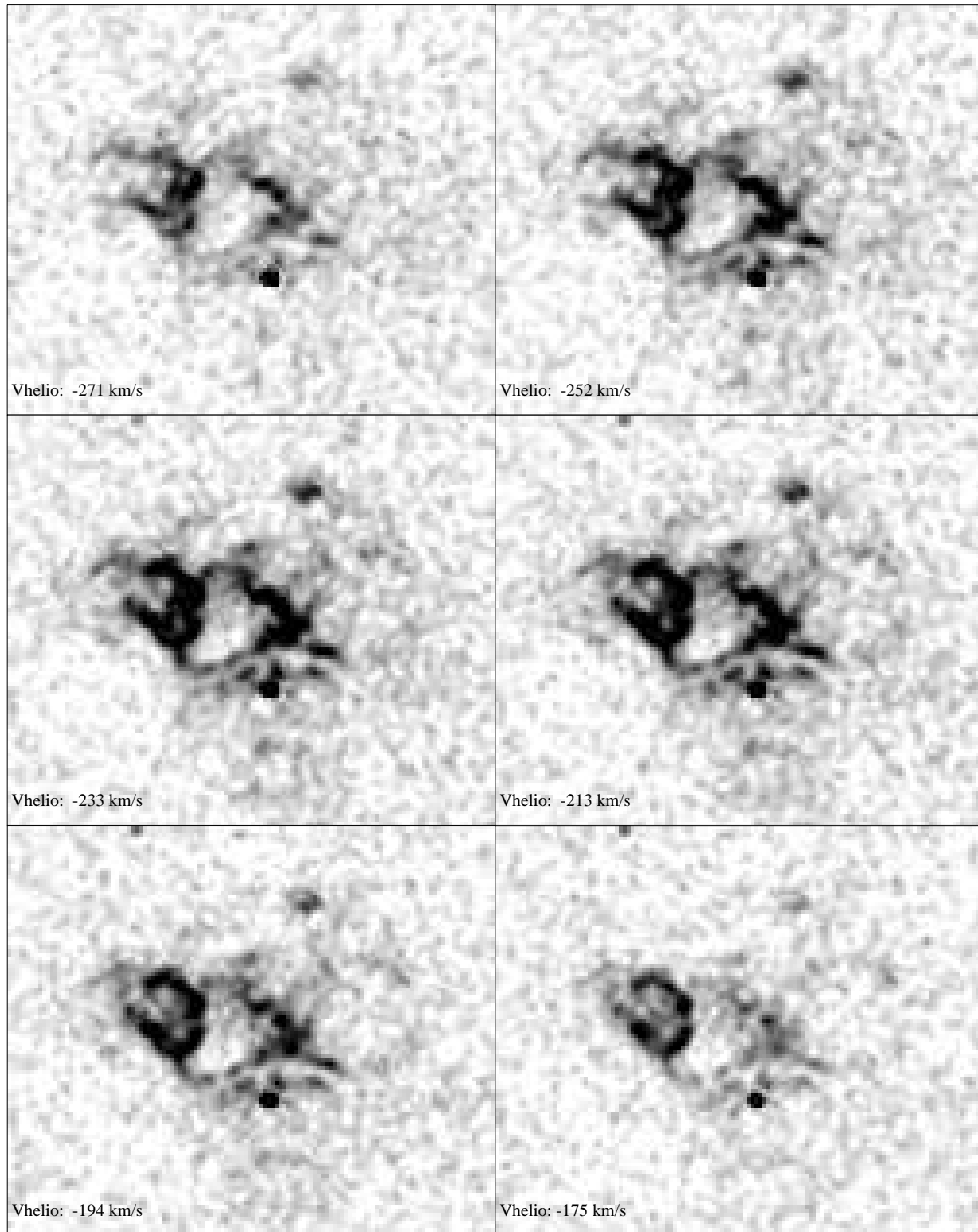


**Fig. 8.** [SII] velocity maps of the NE region in IC 1613 corresponding to the same velocities as in Figure 7. The bright feature to the South corresponds to the SNR Sandage 8.

This relation has been obtained by noting that the kinematic age of wind blown bubbles can be estimated as:  $t = 0.5 - 0.6 R/V$  (McCray 1977).

Table 8 lists the physical parameters of the catalogued superbubbles calculated as discussed above: the superbubble's number (according to our catalogue), the shell radius (see Sect. 5.3), the rms electron density, the expansion ve-

locity, the mechanical energy and the dynamical age of the superbubble. Meaburn et al. (1988) have obtained expansion velocities for five of these superbubbles. Our results agree with these previous observations except for the dimensions of some of the superbubbles.

### 5.3. The diameter distribution of the superbubbles

The angular dimensions of the superbubbles were determined on the velocity maps at  $H\alpha$  and they are given in column 3 in Table 6. The reported dimensions in this table correspond to the extension of the semiaxes in arc sec. In the cases where we have two different values, i.e., when the shell is not circular, we average them. The resulting linear radii are listed in column 2 in Table 8.

Comparing the size distribution of the H II regions and H II complexes of IC 1613 (see Section 4.2) against the superbubble size distribution we note the following differences: while the diameters of the H II regions range from 27 to 254 pc (this later value corresponds to large H II complexes not ring-shaped), those of the superbubbles range from 110 to 304 pc (note that there is an overlap between these two populations). Thus, the superbubbles have, in general, larger dimensions than those of H II regions, pointing towards a more evolved nebular population. Figure 11 shows the size distribution,  $N(R) - R$ , of the superbubbles in IC 1613. It is worth comparing this size distribution with the size distributions of other galaxies. In order to do so, we have examined the size distributions of the galaxies SMC, Holmberg II, M31 and M33 reported in Oey & Clarke (1997; see their Figures 3 and 4). It is important to take into account the small number statistics of the superbubbles in the studied field of IC 1613 (only 17). Furthermore, our superbubbles are ionized regions while the superbubbles in Oey & Clarke (1997) correspond to H I holes. Nevertheless, we see that the distributions show some similarity. The peak of maximum frequency of the superbubbles in these galaxies corresponds to  $D \approx 80$  pc (SMC), 120 pc (M33), 180 pc (M31) and 500 pc (Hol II); this peak, in the case of IC 1613, is at  $\approx 100 - 140$  pc, thus, similar to the one of M 33 H I holes. On the other hand, there is a difference in the maximum linear extent of the superbubbles: the superbubbles in IC 1613 reach  $D \approx 300$  pc while the superbubbles in the other studied galaxies reach diameters of 720 pc (M31), 760 pc (SMC), 1160 pc (M33) and 1400 pc (Hol II); note that the latter two values fall into the category of supershells according to the typical terminology. This difference could be due to the fact that we are only detecting ionized shells while the other studies are based on H I holes. We have also obtained the cumulative diameter distribution  $N(> D)$  for the superbubbles. In Figure 12 we plot  $\log N(> D)$  vs  $D$ . For the superbubbles of IC 1613 a least squares fit gives  $D_0 = 91.84 \pm 3$  pc. This value is in agreement with the value ( $D_0=83$  pc) determined

by Price et al. (1990) who included some superbubbles in their calculation of the diameter distribution.

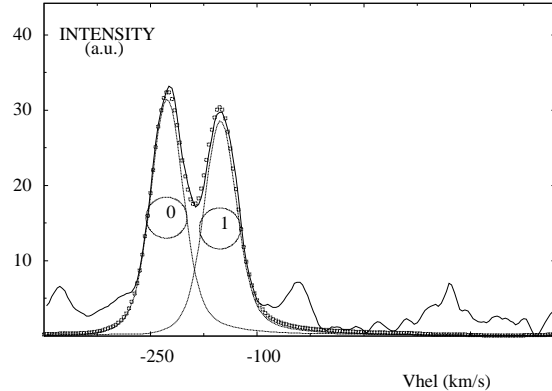


**Fig. 9.** Radial velocity profile of one region of superbubble R2 catalogued in Table 6 and its decomposition in two Gaussian functions, (0) and (1) with peak radial velocities of  $-244$  and  $-147$   $\text{km s}^{-1}$ , respectively, for this particular case. The horizontal axis plots the heliocentric radial velocity while the vertical axis corresponds to the intensity (in arbitrary units). The low velocity peaks correspond to night-sky lines mixed with diffuse emission.

### 5.4. Discussion

We have seen in the preceding sections (more precisely in Section 5.1) that every superbubble detected in this work corresponds to one (or several) stellar association(s) interior to the superbubble. This suggests that the superbubbles are formed by the combined action of stellar winds and supernova explosions of the massive stars of the associations. In what follows, we will examine in more detail this possibility and the models used to describe this formation and evolution.

The shell formation and evolution as a result of the interaction of strong winds of a massive star with its ambient medium has been studied a long time ago by several authors (Dyson & de Vries 1972; Castor et al. 1975; Steigman, Strittmatter & Williams 1975; Weaver et al. 1977, amongst others). The more favored (and complete) description of this interaction is the “standard model” (Weaver et al. 1977) which considers that a star at rest releases a *constant* wind power,  $L_W$ , that interacts with the ambient medium (assumed to be homogeneous). As a result of this interaction, two shocks are formed (one in the stellar wind and another in the ambient medium). The shell formation is the result of these shocks and the shell expansion is driven by the thermal pressure of the shocked stellar wind. The shocked stellar wind has no significant radiative cooling and for this reason this model is also called *adiabatic* or *energy conserving*. This model could also be applied to explain the formation of larger

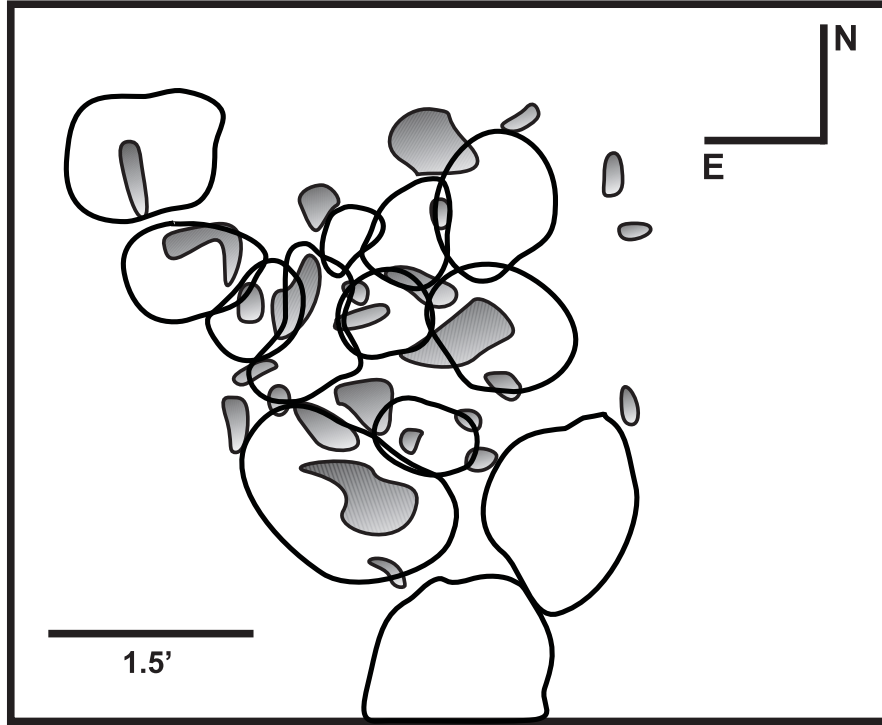


**Fig. 10.** Sketch of the stellar associations studied in Paper I (shaded regions). We have superimposed on this some of the superbubble boundaries already shown in Figure 6. The scale and the orientation are indicated down to the left and top to the right, respectively.

shells (superbubbles and supershells) formed by the combined action of stellar winds and supernova explosions. In spite of the popularity and theoretical simplicity of the standard model, several observational difficulties have prevented its test in real cases. The main difficulty is the poor knowledge of the interior stars and of their wind power. Observational works (Oey 1996b) where the stellar content has been thoughtfully analyzed and using numerical (instead of the analytical) models that take into account the temporal variations of the wind power as a result of the stellar evolution (Oey 1996a), have found discrepancies between the predicted shell radius and expansion velocity in the sense that the expansion velocities are too high for the observed radii (“dynamical discrepancy”) or between the shell radius and velocity and the wind power,  $L_W$ , and pre-shock density,  $n_0$ , in the sense that  $L_W/n_0$  seems to be overestimated by a factor of 10 (“growth rate discrepancy”). Having these considerations in mind we will proceed to analyze our results, summarized in Table 8.

A close examination of the physical parameters reported in Table 8 shows that:

- The rms electron densities of the superbubbles are quite low (from 0.3 to up to  $6.3 \text{ cm}^{-3}$ ). This makes it quite difficult to obtain electron densities from [S II] line-ratio diagnosis because the line-ratios will fall in the low density regime ( $n_e < 300 \text{ cm}^{-3}$ ).

- The  $H\alpha$  luminosities of the superbubbles vary from  $2.11 \times 10^{36}$  to  $5.89 \times 10^{37} \text{ erg s}^{-1}$ . These luminosity values imply a number of ionizing photons  $\text{s}^{-1}$  ranging from  $1.55 \times 10^{48}$  to  $4.33 \times 10^{49}$ . These ionizing photons can be easily supplied by the interior blue stars. Thus, the superbubbles seem to be ionized by the stars of the interior associations.

- The dynamical ages of the superbubbles (column 6 of Table 8) are of the order of 1-2 Myr and in every case, shorter than the age of the interior stellar association (column 4 of Table 5). The fact that the dynamical ages are shorter than those of the stellar associations suggests that the stellar associations could form the superbubbles. Furthermore, the fact that there is a delay (of about 10 Myr) between the formation of the stellar association and the formation of the superbubble (estimated by its dynamical age), suggests that only the most massive stars of the interior association are responsible for superbubble formation when they evolve into supergiants (or perhaps have exploded as supernovae).

- The obtained expansion velocities of the superbubbles are in general quite high. All the known expansion velocities are larger than  $25 \text{ km s}^{-1}$  and there are two superbubbles with expansion velocities larger than  $40 \text{ km s}^{-1}$ . This is similar to the case of the superbubbles in the LMC where Rosado et al. (1981; 1982), Rosado (1986) and Oey (1996a) have found several superbubbles with high expan-

sion velocities. The kinematics of this class of superbubbles (“high velocity superbubbles”) cannot be explained in terms of the “standard model” of adiabatic wind-blown bubbles (Weaver et al. 1977) because the expansion velocities are too large for the observed shell radius, according to the predictions of this model.

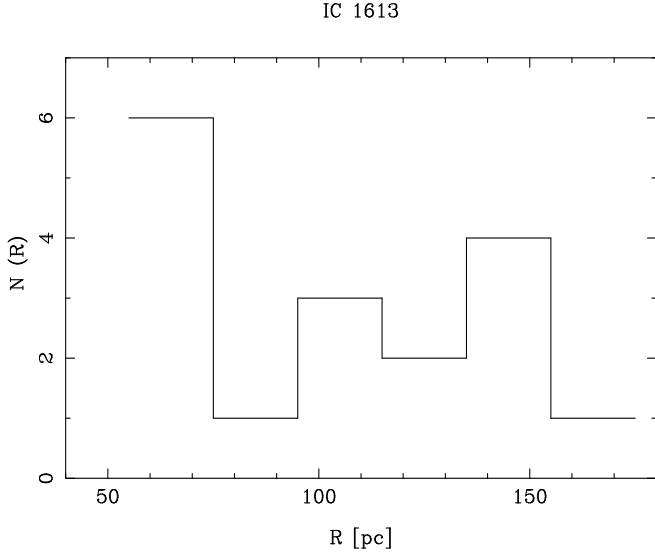


**Fig. 11.** Size distribution function,  $N(R) - R$ , for the superbubbles in IC 1613.

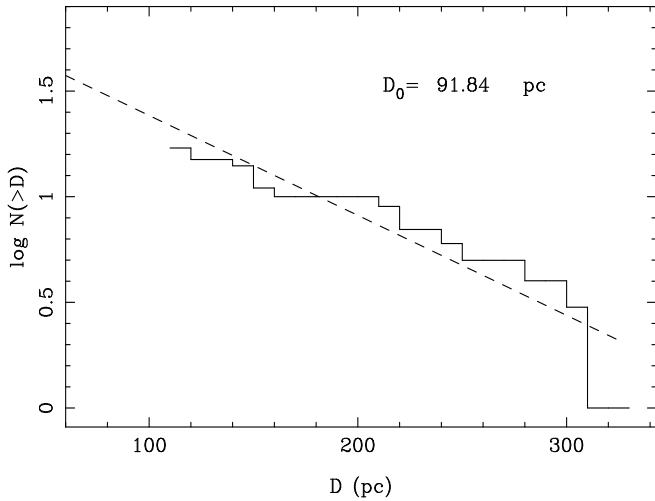


**Fig. 12.** The cumulative size distribution for the superbubbles in IC 1613. The dashed straight line is a least square fit. The value for the characteristic diameter is given to the right.

In the case of the superbubbles of IC 1613, our stellar photometry can give us some knowledge of the massive stars interior to the catalogued superbubbles but we can-

not follow the treatment given in Oey (1996a) because further spectroscopic work is needed in order to know accurately the content of massive stars. In the absence of this accurate knowledge we can, nevertheless, estimate the required wind power ( $L_W$ ) of each superbubble and compare it with the number of massive stars that we detect in our photometric observations, in order to see, in terms of energy considerations, whether the standard model could explain the superbubble formation.

Assuming that the superbubbles evolve according to the standard model of wind-blown bubbles (Weaver et al. 1977), the wind power,  $L_W$ , released by the stars *constantly during all* of the dynamical age of the shell is given by:

$$L_W = 3.2 \times 10^{-7} n_0 (\text{cm}^{-3}) V_{\text{EXP}}^3 (\text{km s}^{-1}) R^2 \times 10^{36} \text{ ergs s}^{-1}$$

where,  $n_0$ , the ambient pre-shock density, is taken as:  $n_0 = n_e / 4$  by assuming that the swept-up mass in the shell comes from a homogeneous sphere of radius  $R$ . Both  $n_e$  and  $R$  are listed in Table 8.

A wind power of  $4 \times 10^{36} \text{ ergs s}^{-1}$  is reasonably expected for one O9.5 or B0 supergiant star (Pauldrach et al. 1986) during its lifetime in this phase (about  $10^6 \text{ yr}$ ). More massive stars can have larger wind powers but the duration of those phases is ten times shorter. That is the case for O4I stars that can release more than 100 times the wind power of  $1 \times 10^{36} \text{ ergs s}^{-1}$ , or of WR stars that can release about  $50 \times 10^{36} \text{ ergs s}^{-1}$ ; however, these events occur only during time scales shorter than the dynamical ages of the superbubbles considered here (a few  $10^5 \text{ yr}$  compared with the dynamical ages of about 1 Myr derived in this work).

In Table 9 we list the required wind power  $L_W$  that can explain the observed expansion velocities and radii of the superbubbles studied here, in terms of the standard model, and the number of detected blue stars (with  $M_V < -2$ , or  $M_* > 7 M_\odot$ ),  $N_B$ , quoted in column 3 of Table 7. We see that superbubbles with expansion velocities lower than  $30 \text{ km s}^{-1}$  have wind powers that are easily explained by the number of blue stars inside them (assuming that they are all supergiants and earlier than B0). On the contrary, there are some extreme cases, such as R2, where the required wind power seems to imply that some of the interior blue stars should release much more powerful winds. Given our limitations in the accurate knowledge of the stellar content of the superbubbles, we can only state that, from energy considerations, the superbubbles studied here could be formed by the stellar winds of the interior stars.

It is interesting to note from Table 6 that the superbubbles of IC 1613 with higher velocities seem to be brighter in [S II] emission. On the other hand, an inspection of Table 8 shows that all the superbubbles have mechanical energies of at most 80 % the energy of one supernova explosion (approximately  $1-3 \times 10^{51} \text{ ergs}$ ). Taking into account that between 20 to 30 % of this energy is

transmitted to the ambient medium as kinetic energy, one or two SN explosions could also account for the formation (or acceleration) of the superbubbles. However, no traces of these SN explosions (such as extended X-rays sources or non-thermal radio emission) have been found.

## 6. The velocity field of IC 1613

Figure 13 shows the global radial velocity field (not corrected for projection effects) of the central region of IC 1613 obtained from our FP data in  $H\alpha$ , considering diffuse gas, H II regions and superbubbles. In this map a chaotic distribution of velocities across the galaxy can be seen: some local events are superimposed onto the regular field. These local events are the peculiar kinematical signatures of the superbubbles, which are notorious. However, when the expansions are extracted, we see a variation in the mean velocities across the field. Along the NE region, a gradient of velocities ranges from  $-210 \text{ km s}^{-1}$  in the southeast to  $-250 \text{ km s}^{-1}$  in the northwest. The extreme detected velocities are due to the contamination of the superbubble and SNR internal motions. Indeed, the region N27 (with the maximum velocity of  $-139 \text{ km s}^{-1}$ ) is the superbubble R2 and N18 (with the minimum velocity of  $-328 \text{ km s}^{-1}$ ) is the SNR Sandage 8. It would be important to have kinematic data of the ionized gas over the whole dimensions of this galaxy in order to obtain its rotation curve.

On the other hand, in Figure 14, the 21-cm isovelocities from Lake & Skillman (1989) are sketched together with the radial velocity distribution of the H II regions, obtained in this work. Their velocity resolution is  $6.18 \text{ km s}^{-1}$  and the linear resolution is approximately 210 pc. In this figure we can see that in general, the optical distribution does not correspond to any particular kinematical H I feature. However, with respect to the density distribution (not shown), it has been noted that the optical extent of IC 1613 is located at the peak of the H I density distribution and at the ridge of an H I hole (Lake & Skillman 1989). In order to compare the kinematics of the ionized gas with the H I kinematics we also require more observations covering the whole optical extent of this galaxy.

## 7. Conclusions

We have measured – by means of a Fabry-Perot interferometer – the kinematical parameters of the H II regions that we have detected within the  $10'$  field of view of our observations (which includes most of the optical emission of IC 1613). We found that the H II regions of IC 1613 present similar integrated properties as well as  $H\alpha$  line profiles with simple structure that are fitted by single Gaussian curves. We obtained also the  $H\alpha$  fluxes and luminosities of these H II regions. The luminosity function of these H II regions can be fitted to a power law function of slope  $a = -1.54 \pm 0.1$  in agreement with the value given

by HLG. We have also studied the diameter distribution and the cumulative diameter distribution of the H II regions within our field of view. We obtained a characteristic diameter  $D_0 = 65.41 \pm 3 \text{ pc}$  which is slightly larger than the previous determination by HLG, probably because our field is smaller. Our characteristic diameter value does not seem to follow the correlation found by Hodge (1983) between  $D_0$  and the absolute magnitude  $M_B$  for a sample of irregular galaxies.

We have also found that the ISM of the entire galaxy is organized in a complex network of superbubbles. We have catalogued the superbubbles detected in our field of view. We have also calculated the 2-D porosity parameter,  $Q_{2D}$ , in the field of view of our observations and seen that the  $Q_{2D}$  value is intermediate between the observed values for the SMC and M31.

Most of the superbubbles that we have detected show complex radial velocity profiles (some others are so faint that we cannot measure line-splitting in their velocity profiles). These kind of profiles along the same nebula are indicative of internal gas motions and expansions. We have determined the expansion velocities and other physical parameters of the superbubbles found in this work. In addition, we have used the photometric data published in a previous work (Paper I) and in Hodge (1978) in order to know the stellar content of the catalogued superbubbles. We find that almost every superbubble has an interior association containing massive stars, suggesting a physical link between them. Furthermore, we find that the dynamical time scales of the superbubbles are always shorter than the ages of the interior stellar associations. The mean temporal delay between those ages (about 10 Myr) suggests that only evolved members (i.e., the more massive stars) of these associations are responsible for the formation of the superbubbles, possibly when they evolve to supergiants or when they explode as supernovae.

We have found that all the superbubbles with measured expansion velocities have expansion velocities larger than  $25 \text{ km s}^{-1}$ . We used energy considerations in order to explain the origin of the superbubbles in terms of stellar winds and supernova explosions. We find that the superbubbles with extreme expansion velocities (larger than  $36 \text{ km s}^{-1}$ ) require interior stars with winds much more powerful than the average of B0–O9.5 supergiant stars if they are wind blown shells following the “standard model”. On the other hand, one or two supernova explosions could explain the mechanical energies involved. However, no other traces of SN explosions (extended X-rays, non-thermal radio emission) are known for these superbubbles except an enhancement of their [S II] emission.

We have obtained the size distribution and the cumulative diameter function of superbubbles detected in our field of view and compared these size distributions with size distributions of superbubbles in other galaxies. Our results are statistically poor. However, the value of the characteristic diameter we obtain,  $D_0 = 91.84 \pm 3 \text{ pc}$ , is

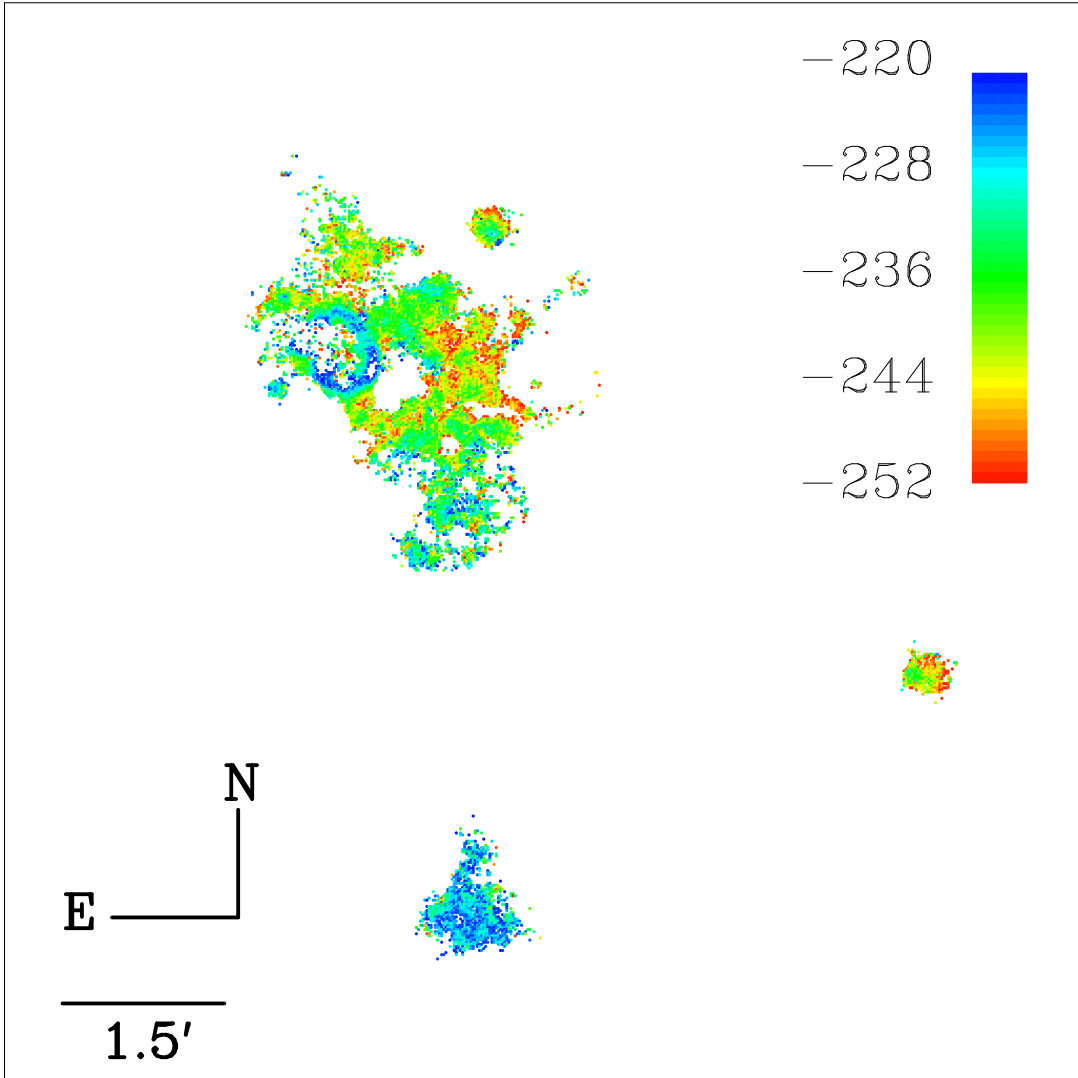


**Fig. 13.** IC 1613  $H\alpha$  observed radial velocity distribution (see text for details). The colors are related to velocities given in  $\text{km s}^{-1}$ . The scale and the orientation are indicated to the left.

in agreement with the value given by Price et al. (1990) for the nebulae in this galaxy.

On the other hand, we have determined the global  $H\alpha$  velocity field of IC 1613, inside our  $10'$  field of view. The velocity field is contaminated by the internal motions of the superbubbles of this galaxy. Nevertheless, a gradient of velocities is suggested across the SE-NW direction. In addition, we compare the mean velocities obtained from the H II regions with the kinematics of the H I gas but we do not find a clear agreement between them.

*Acknowledgements.* The authors wish to thank Drs. I. Puerari, D. Mayya, A. Luna and O. López-Cruz, for their comments and criticism about this work, and Mrs. J. Benda for the revision of the final version. MVG thanks support from a CONACyT scholarship under register number 114735. This work was partially supported by the grants IN122298 of DGAPA-UNAM and 27984-E of CONACYT.

This research used the NASA/IPAC Extragalactic Database (NED) which is operated by the Jet Propulsion Laboratory, California Institute of Technology, under contract with the National Aeronautics and Space Administration.

## References

- Armandroff, T.E, Massey, P. 1985, ApJ 291, 685
- Azzopardi M., Lequeux, J., Maeder, A. 1988, A&A 189, 34
- Baade, W. 1963, The evolution of stars and galaxies (Harvard University, Cambridge)
- Castor, J., Weaver, R., McCray, R. 1975, ApJ 200, L107
- de Vaucouleurs, G., de Vaucouleurs, A., Corwin, H. G. 1976, 2nd Ref. Cat. of Bright Galaxies
- Dickel, J.R., D'odorico, S., Silverman, A. 1985, AJ 90, 414
- d'Odorico, S., Dopita, M. A., Benvenuti, P. 1980, A&AS 40, 67
- d'Odorico, S., Rosa, M. 1982, A&A 105, 410

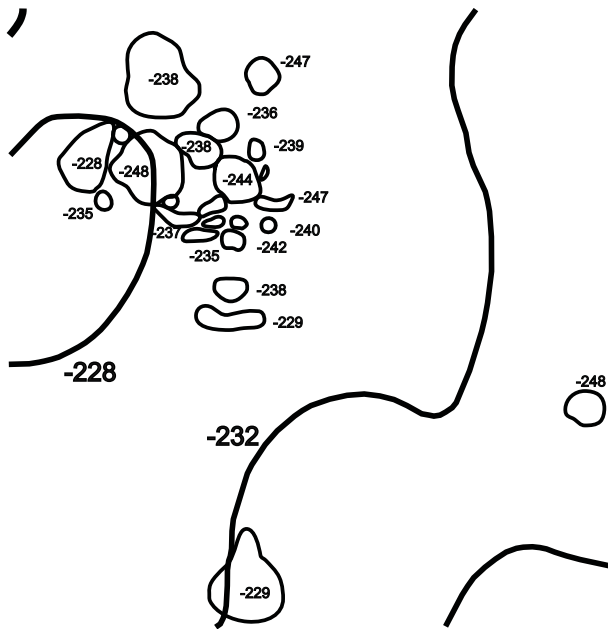


**Fig. 14.** IC 1613 H $\alpha$  observed radial velocity distribution. Heavy lines correspond to H I isovelocities (Lake & Skillman 1989).

Dyson, J. E., de Vries, J. 1972, A&A 20, 223  
 Freedman, W. 1988a, ApJ 326, 691  
 Freedman, W. 1988b, AJ 96, 1248  
 Georgiev L., Borissova, J., Rosado, M., et al., 1999, A&AS 134, 21 (Paper I)  
 Goss, W. M., Lozinskaya, T. A. 1995, ApJ 439, 637  
 Hippelein, H. H. 1986, A&A 160, 374  
 Hodge P. W. 1978, ApJS 37, 145  
 Hodge P. W. 1980, ApJ 241, 125  
 Hodge, P. W. 1983, AJ 88, 1323  
 Hodge, P. W., Lee, M. G., Kennicutt, R. C. 1989, PASP 101, 32  
 Hodge, P. W., Lee, M.G., Gurwell, M. 1990, PASP 102, 1245 (HLG)  
 Hunter, D., Hawley, W.N., Gallagher, J.S. 1993, AJ 106, 1797 (HHG)  
 Huchtmeier, W. K., Seiradakis, J.H., Materne, J. 1981, A&A 102, 134  
 Kennicutt, R. C., Edgar, B. K., Hodge, P. W. 1989, ApJ 337, 761  
 Kingsburgh, R. L., McCall, M. L. 1998, AJ 116, 2246  
 Kingsburgh, R. L., Barlow, M. J. 1995, A&A 295, 75  
 Lake, G.R., Skillman, E.D. 1989, AJ, 98, 1274  
 Le Coarer, E., Rosado, M., Georgelin, Y., et al., 1993, A&A 280, 365  
 Lequeux, J., Meysonnier, N., Azzopardi, M. 1987, A&AS 67, 169  
 Martín, M. C. 1998, A&AS 131, 77  
 Mateo, M. L. 1998, ARA&A 36, 435  
 McCray, R. 1977, Astrophysics and Space Science Library, 70, 35  
 Meaburn, J., Clayton, C. A., Whitehead, M.J. 1988, MNRAS 235, 479

Oey, M. S. 1996a, ApJ 467, 666  
 Oey, M. S. 1996b, ApJS 104, 71  
 Oey, M. S., Clarke, C. J. 1997, MNRAS 289, 570  
 Parker, J. Wm., Hill, J. K., Bohlin, R. C., et al., 1996, ApJ 472, L29  
 Pauldrach, A., Puls, J., Kudritzki, R. P. 1986, A&A 164, 86  
 Peimbert, M., Bohigas, J., Torres-Peimbert, S. 1989 Rev. Mex. Astron. astrofis. 16, 45  
 Price, J.S., Mason, S.F., Gullixson, C.A. 1990, AJ 100, 420  
 Roberts, M. S. 1972, in External Galaxies and Quasi-stellar Objects (IAU Symposium 44), Ed. Evans, Wills and Wills, p. 12  
 Rosado, M., Georgelin, Y.P., Georgelin, Y.M., et al. 1981, A & A 97, 342  
 Rosado, M., Georgelin, Y.M., Georgelin, Y.P., et al. 1982, A & A 115, 61  
 Rosado, M. 1986, A&A 160, 211  
 Rosado, M., Langarica, R., Bernal, A., et al. 1995, Rev. Mex. Astron. Astrof. Conf. Ser. 3, 268  
 Rosado, M., Laval, A., Le Coarer, E., et al., 1996, A&A 308, 588  
 Rosado, M., et al., in preparation  
 Sandage, A. 1971, ApJ 166, 13  
 Sandage, A., Katem, B. 1976, AJ 81, 743 (Washington:NASA), p.263  
 Spitzer, L. Jr.: 1978, Physical Processes in the Interstellar Medium, J. Willey & Sons, New York.  
 Steigman, G., Strittmatter, P.A., Williams, R.E. 1975, ApJ 198, 575  
 Strobel, N.V., Hodge, P.W., Kennicutt, R.C. 1991, ApJ 383, 148  
 van den Bergh, S. 1981, AJ 86, 1464  
 Weaver, R., Mc Cray, R., Castor, J., et al. 1977, ApJ 218, 377  
 Youngblood, A., Hunter, D. 1999, ApJ 519, 55



**Table 1.** IC 1613 properties

Name	IC 1613
Type <sup>a</sup>	IB(s)m
R.A (1950) <sup>a</sup>	01h02m11.8s
Dec (1950)	+01d51m00s
B magnitude <sup>a</sup>	9.88
Angular size (arcmin) <sup>a</sup>	16.2× 14.5
Heliocentric radial velocity (km s <sup>-1</sup> ) <sup>b</sup>	-237
Distance (kpc) <sup>c</sup>	725
Inclination (degrees) <sup>b</sup>	30
P.A (degrees) <sup>b</sup>	50

<sup>a</sup> NED<sup>b</sup> Optical heliocentric radial velocity from Martín (1998)<sup>c</sup> Adopted distance in this work, based on Freedman (1988a, 1988b)**Table 2.** Parameters of the FP Interferometric Observations

Instrument	PUMA	
Detector	TEKTRONIX CCD	
FP Scanning Steps	48	
Finesse	24	
Filters	H $\alpha$	[S II]
Central Lambda (Å)	6570	6720
Interference order	330	322
Free spectral range (km s <sup>-1</sup> )	847	931
Sampling resolution (km s <sup>-1</sup> /channel)	18.9	19.4
Calibration line	6562.78 H	6717.04 Ne
Binning	2×2	4×4
Final pixel size (arcsec)	1.17	2.34

**Table 3.** HLG HII regions taken for calibration

Sandage <sup>a</sup> ID	HLG <sup>b</sup> ID	F <sup>c</sup>	S <sup>d</sup>	Counts <sup>e</sup>	Counts per sr <sup>f</sup>
S2	13	220	1.20	27727	1.51
S18	31	131	1.57	15584	2.00
S6	36	108	1.84	26873	4.72
S16	46f	63	5.90	12398	10.42
–	46g	39	3.47	8721	7.33
–	59	45	0.66	7729	1.12
–	67c	105	5.06	15884	7.16
S11	70	26	2.09	3489	2.93

<sup>a</sup> Sandage identification (Sandage 1971).<sup>b</sup> HLG identification (Hodge et al. 1990).<sup>c</sup> HLG published H $\alpha$  fluxes, in units of  $10^{-15}$  erg cm<sup>-2</sup> s<sup>-1</sup>.<sup>d</sup> Surface brightness derived from HLG fluxes, in units of  $10^{-5}$  erg cm<sup>-2</sup> s<sup>-1</sup> sr<sup>-1</sup>.<sup>e</sup> Counts (sky subtracted) in our image integrated over the areas defined by HLG.<sup>f</sup> In units of  $10^{12}$  counts sr<sup>-1</sup>.

**Table 4.** Measured parameters for H II regions in IC 1613

Source <sup>a</sup>	Sandage <sup>b</sup>	HLG <sup>c</sup>	D <sup>d</sup>	$V_1$ <sup>e</sup>	$V_2$	$\sigma_1$ <sup>f</sup>	$\sigma_2$	$\log F(\text{H}\alpha)$ <sup>g</sup>	$\log L(\text{H}\alpha)$ <sup>h</sup>
N1	S2	13	127.6	-248		20.0		-12.41	37.34
N2		(25),30	53.3	-242		18.8		-13.50	36.25
N3		26	78.1	-254		31.4		-13.28	36.47
N4		27,(33)	47.2	-242		26.5		-13.72	36.03
N5	S12	29,(35)	80.5	-247		21.2		-12.83	36.91
N6	S18	31,32	99.0	-247		21.2		-12.89	36.86
N7		34	34.2	-244		21.2		-13.53	36.22
N8	S6	36	57.5	-240		12.0		-12.89	36.86
N9	S3**	37	253.6	-229		18.8		-12.14	37.61
N10		38	64.6	-239		18.8		-13.36	36.39
N11	S7	39,40	56.6	-239		10.4		-12.87	36.88
N12		42,59	117.3	-229		21.2		-13.08	36.67
N13		(44)	29.3	(-282)		(5.9)		-14.74	35.01
N14	S17	45	90.8	-236		18.8		-12.79	36.96
N15	<b>S15,S16</b>	<b>46</b>	138.3	-244		22.2		-12.14	37.61
N16		47,57	34.7	-236		17.6		-13.27	36.48
N17		48,58,61	60.1	-235		16.3		-13.09	36.66
N18	S8*	49	34.5	-239	-335	34.3	86.1	-12.54	37.21
N19		50,41	14.0	-242		17.6		-13.61	36.14
N20	S5	51,52,53	93.5	-238		16.3		-13.05	36.70
N21	<b>S14</b>	<b>55</b>	108.1	-238		18.8		-12.63	37.12
N22		56	44.5	-236		22.2		-13.28	36.47
N23		(60)	29.1	-242		22.2		-14.51	35.24
N24		63	26.9	-240		24.4		-13.94	35.81
N25		64	76.3	-237		24.4		-12.87	36.88
N26		66	184.5	-238		21.2		-12.46	37.29
N27	<b>S10,S13</b>	<b>67</b>	198.1	-248	-185	22.2	18.9	-11.98	37.77
N28		<b>69</b>	42.2	-228		29.5		-13.63	36.12
N29	S11	70,73	42.7	-235		22.2		-13.53	36.22
N30		<b>72</b>	99.0	-228		32.4		-13.06	36.69

<sup>a</sup> Identification used in this work.<sup>b</sup> Sandage identification (Sandage 1971). The regions marked in boldface are known superbubbles previously catalogued as H II regions. The asterisks indicate the regions hosting the supernova remnant (a single asterisk) and the Wolf-Rayet star (two asterisks).<sup>c</sup> HLG identification (Hodge et al. 1990). The regions marked in boldface are known superbubbles previously catalogued as H II regions. The regions quoted between parentheses are objects with uncertain identification.<sup>d</sup> Equivalent diameter in parsecs (see text for definition).<sup>e</sup> Peak velocity in units of  $\text{km s}^{-1}$ . Parentheses indicate uncertain values.<sup>f</sup> Velocity dispersion in units of  $\text{km s}^{-1}$ . Parentheses indicate uncertain values.<sup>g</sup> Logarithm of the  $\text{H}\alpha$  flux in units of  $\text{erg cm}^{-2} \text{s}^{-1}$ .<sup>h</sup> Logarithm of the  $\text{H}\alpha$  luminosity in units of  $\text{erg s}^{-1}$ .

**Table 5.** Stellar content of the H II regions in IC 1613

Source	Known stars <sup>a</sup>	Related object <sup>b</sup>	Stellar association <sup>c</sup>	comments	Stellar association <sup>d</sup>	clusters <sup>e</sup>
N1					H5	c32, c41
N2					H10	
N3			G10		H11	
N4			G11			
N5	AM4	O-B	G7	embedded	H10	
N6			G10	center	H11	c13
N7					H13	
N8					H12	
N9	AM6	WO				
N10			G11	center	H13	c14
N11			G14	embedded	H14	c40,c12
N12			G13			
N13						
N14			G19			
N15	AM5	O-B	G16, G17	embedded	H13	c11
N16			G14	embedded	H14	
N17			G18	embedded	H14	
N18	AM8	SNR	G14	embedded	H14	c16
N19			G12,G14	embedded	H14	
N20			G15	center	H15	c18
N21			G17, G21	embedded	H13	c15
N22						
N23						
N24			G24	embedded	H17	
N25			G23, G24	embedded		
N26			G19			
N27			G21, G25, G28	embedded	H17	
N28			G28	embedded		
N29						
N30			G28		H18	

<sup>a</sup> Stars with known spectra: WR candidates from Armandroff & Massey (1985)<sup>b</sup> Spectral types from Azzopardi et al. (1988).<sup>c</sup> Associations determined in Paper I.<sup>d</sup> Associations determined by Hodge (1978).<sup>e</sup> Stellar clusters determined in Hodge (1978) and in Paper I.

**Table 6.** Catalogue of Superbubbles in the galaxy IC 1613

Source	ID <sub>1</sub> <sup>a</sup> (ID <sub>2</sub> ) <sup>b</sup>	axis <sup>c</sup> " × "	V <sub>1</sub> km s <sup>-1</sup>	V <sub>2</sub> km s <sup>-1</sup>	log F(H $\alpha$ ) <sup>d</sup>	log L(H $\alpha$ ) <sup>e</sup>	Comments
R1	GS1a (S13)	39 × 39	-216	-274	-12.23	37.51	High [SII] emission
R2	GS1b (S10)	49 × 33	-244	-147	-11.98	37.77	High [SII] emission
R3	(HIV) (HHG 2)	73 × 59	-238	-179	-12.23	37.52	Faint [SII] emission
R4	GS2 (HHG 1)	66 × 50	-277	-213	-12.18	37.57	Ring of HII regions
R5	GS4 (S15)	33 × 30	-228	-153	-12.10	37.65	High [SII] emission
R6	GS5 (S16+HIII) (HHG 4)	64 × 52	-240	-190	-12.64	37.11	Faint [SII] emission
R7	GS6 (HIV) (HHG 5)	47 × 38	-234	(-174)	-12.72	37.03	
R8	– (HVII) (HHG 3)	63 × 49	-259	-208	-13.08	36.67	
R9	– (H5+S5+S7+S8)	90 × 90	-237	-317	(-12.31)	37.44	Ring of HII regions
R10	– (S6(contained))	37 × 37	-229	(-182)	-12.71	37.04	[SII] detected S8 SNR <sup>f</sup>
R11	–	77 × 77	-205	–	-13.19	36.56	Very faint
R12	– (HII(contained))	108 × 61	-210	-138	-12.69	37.06	
R13	GS3 (S12+S14)	37 × 24	-217	-296	-12.62	37.13	Expansion better seen in [SII]
R14	– (HXII)	85 × 77	-234	–	-13.39	36.36	Very faint
R15	– (HIX)	45 × 35	-254	-199	-13.20	36.55	Very faint
R16	– (D1)	73 × 64	-210	–	-12.89	36.85	Very faint
R17	– (HI contained)	108 × 59	-215	–	-13.43	36.32	

<sup>a</sup> Meaburn et al. (1988) identification.<sup>b</sup> Price et al. (1990) or HHG for Hunter et al. (1993) identifications.<sup>c</sup> Dimensions of the superbubble semiaxis in arcsecond units (see details in section 4.2).<sup>d</sup> Flux logarithm in units of erg cm<sup>-2</sup> s<sup>-1</sup>.<sup>e</sup> Luminosity logarithm in units of erg s<sup>-1</sup>.<sup>f</sup> S8 SNR projected at the boundary of this superbubble.

**Table 7.** Stellar Content of the Superbubbles in the galaxy IC 1613

Source	Paper I Hodge (1978)	$N_B$	Age (Myr)	Known stars	Blue SG	$\Gamma$
R1	part of G28 H18	3	20	no	no	-2.4 +/- 0.3
R2	G25, part of G28 H17	17	8	no	one (B0)	-1.6 +/- 0.2
R3	G29 H19	8	20	no	no	-2.1 +/- 0.1
R4	parts of G16, G17, G21, G24, G25 H13, H17 (parts of)	37	8–10	no	no	-1.6 +/- 0.2
R5	part of G16 H13 (part of)	7	10	one (OBem(?))	one (S13)	-1.7 +/- 0.2
R6	G5, G7, G11 H10, H13 (part of)	36	5	one (OB)	two (cB1.5, A0Ia)	-1.3 +/- 0.3
R7	G9, part of G11 H13 (part of)	16	10	no	no	-1.7 +/- 0.2
R8	parts of , G9, G10	5	–	no	one (B2I)	–
R9	G12, G14, G15, G18, part of G6, G13 H14, H15	106	5–10	no	no	-2.0 +/- 0.2
R10	G8, part of G12 part of H14	7	5	no	one	-1.1 +/- 0.2
R11	–	–	–	–	–	–
R12	–	–	–	–	–	–
R13	part of G21 part of H17	9	8	no	no	-1.6 +/- 0.2
R14	– H6, H5	21	16	no	no	–
R15	– H4	36	31	no	no	–
R16	– H8	8	24	no	no	–
R17	– H9	25	11	no	no	–

**Table 8.** Physical Parameters of the Superbubbles in the galaxy IC 1613

Source	R	$n_e(\text{rms})$	$V_{EXP}$	K.E <sup>a</sup>	$t^b$
	pc	$\text{cm}^{-3}$	$\text{km s}^{-1}$	ergs	Myr
R1	70	3.8	29	1.88	1.2
R2	74	4.9	49	8.07	0.7
R3	119	1.8	30	4.64	1.9
R4	105	2.2	32	4.49	1.6
R5	55	6.3	38	2.56	0.7
R6	105	1.4	25	1.70	2.0
R7	77	1.9	(30)	(1.34)	(1.2)
R8	101	0.8	26	1.01	1.9
R9	162	(1.1)	–	–	–
R10	66	2.4	(24)	(0.69)	(1.3)
R11	138	0.4	–	–	–
R12	152	0.7	36	5.75	2.0
R13	55	3.6	32	1.04	0.8
R14	146	0.3	–	–	–
R15	72	1.3	28	0.64	1.2
R16	123	0.7	–	–	–
R17	150	0.3	–	–	–

<sup>a</sup> Mechanical energy in units of  $10^{50}$  ergs. See section 5.2 for details.

<sup>b</sup> Dynamical age in units of Myrs. See section 5.2 for details.

**Table 9.** Comparison between the predicted wind power and the detected blue stars for the superbubbles of IC 1613

Source	$L_W^a$	$N_B^b$
R1	36	3
R2	253	17
R3	55	8
R4	64	37
R5	84	7
R6	19	36
R7	24	16
R8	11	5
R9	–	106
R10	12	7
R11	–	–
R12	60	–
R13	29	9
R14	–	21
R15	12	36
R16	–	8
R17	–	25

<sup>a</sup> Predicted wind power in units of  $10^{36}$  ergs  $\text{s}^{-1}$ . See section 5.4 for details.

<sup>b</sup> Observed blue stars. See section 5.4 for details.

This figure "ms9979f1.gif" is available in "gif" format from:

<http://arxiv.org/ps/astro-ph/0010556v1>

This figure "ms9979f6.gif" is available in "gif" format from:

<http://arxiv.org/ps/astro-ph/0010556v1>